Evaluation of the effects of nanoprecipitation process parameters on the size and morphology of poly(ethylene oxide)-block-polycaprolactone nanostructures

Känkänen, Voitto

2020-11-30

Känkänen , V , Seitsonen , J , Tuovinen , H M , Ruokolainen , J , Hirvonen , J , Balasubramanian , V & Santos , H A 2020 , ' Evaluation of the effects of nanoprecipitation process parameters on the size and morphology of poly(ethylene oxide)-block-polycaprolactone nanostructures ' , International Journal of Pharmaceutics , vol. 590 , 119900 . https://doi.org/10.1016/j.ijpharm.2020.119900

http://hdl.handle.net/10138/334641
https://doi.org/10.1016/j.ijpharm.2020.119900

Evaluation of the effects of nanoprecipitation process parameters on the size and morphology of poly(ethylene oxide)-*block*-polycaprolactone nanostructures

Voitto Känkänen[a], Jani Seitsonen[b], Henri Tuovinen[a], Janne Ruokolainen[b], Jouni Hirvonen[a], Vimalkumar Balasubramanian[c]*, Hélder A. Santos[a,d]*

[a] Drug Research Program, Division of Pharmaceutical Chemistry and Technology, Faculty of Pharmacy, University of Helsinki, FI-00014 Helsinki, Finland

[b] Nanomicroscopy Center, Aalto University, Puumiehenkuja 2, FI-02150 Espoo, Finland

[c] Chemical and Pharmaceutical Development, Bayer Oy, FI-20210 Turku, Finland

[d] Helsinki Institute of Life Science (HiLIFE), University of Helsinki, FI-00014 Helsinki, Finland

*Corresponding author

E-mail address: helder.santos@helsinki.fi (H.A. Santos), vimalkumar.balasubramanian@bayer.com (V. Balasubramanian)

Keywords:

Block copolymers; Nanoparticles; Self-assembly; Nanoprecipitation; Statistical models; Process optimization

Abstract:

Nanoprecipitation is a straightforward method for the production of block copolymer nanoparticles for drug delivery applications. However, the effects of process parameters need to be understood to optimize and control the particle size distribution (PSD). To this end, we investigated the effects of material and process factors on PSD and morphology of nanoparticles prepared from an amphiphilic diblock copolymer, poly(ethylene oxide)-*block*-polycaprolactone. Using a Design of Experiments approach, we explored the joint effects of molecular weight, block length ratios, water volume fraction, stirring rate, polymer concentration and organic phase addition rate on hydrodynamic size and polydispersity index of the nanostructures and created statistical models explaining up to 94 % of the variance in hydrodynamic diameter. In addition, we performed morphological characterization by cryogenic transmission electron microscopy and showed that increasing the process temperature may favor the formation of vesicles from these polymers. We showed that the effects of process parameters are dependent on the polymer configuration and we found that the most useful parameters to fine-tune the PSD are the initial polymer concentration and the stirring rate. Overall, this study provides evidence on the joint effects of material and process parameters on PSD and morphology, which will be useful for rational design of formulation-specific optimization studies, scale-up and process controls.

Introduction

Nanoparticles (NPs) prepared from amphiphilic block copolymers (BCPs) have been the subject of intense study in the last three decades. Widespread interest in BCP NPs results from their attractive properties, such as high colloidal stability, synthetic tailorability, and ease of preparation via simple bottom-up type processes based on molecular self-assembly. One of the major application areas for BCP NPs is their use as colloidal drug delivery vehicles and such systems have already reached the clinics (Anselmo and Mitragotri 2019; Bobo, et al. 2016; Werner, et al. 2013).

Amphiphilic BCPs have the ability to assemble, in aqueous solutions, into aggregates of various morphologies, such as spherical micelles, worm-like micelles and vesicles (polymersomes). This microphase separation is due to the mutual repulsion between the constituent blocks and for a given polymer structure, the thermodynamic equilibrium morphology is essentially determined by the relative volumes occupied by the two blocks (Discher and Ahmed 2006; Mai and Eisenberg 2012), commonly expressed by the hydrophilic volume fraction, f. However, the morphology is also heavily influenced by the NP manufacturing method and parameters, such as solvent and temperature, as the polymer chains can be trapped into kinetically (meta)stable morphologies (Hayward and Pochan 2010).

In drug delivery applications, poly(ethylene oxide) is by far the most widely used polymer for the hydrophilic block (Adams, M. L., et al. 2003). Common choices for the hydrophobic block include degradable polyesters, such as poly(lactic acid), poly(glycolic acid), poly(lactic-co-glycolic acid) and poly(ε-caprolactone) (PCL), of which PCL shows the slowest degradation (Adams, M. L., et al. 2003; Woodruff and Hutmacher 2010). The diblock poly(ethylene oxide)-*block*-polycaprolactone (PEO-*b*-PCL) and slight variations thereof have been used as a carrier material for various active ingredients and imaging agents in the form of solid NPs (Ali, et al. 2017; Allen, et al. 1998; Deng, et al. 2014; Dong, et al. 2010; Gref, et al. 1994; Lim Soo, et al. 2005; Liu, J. and Gan 2014; Montazeri Aliabadi, et al. 2005; Park, Y. J., et al. 2002; Patel, et al. 2009; Ryu, et al. 2000; Shi, et al. 2005; Villamil, et al. 2019) or vesicles (Ahmed and Discher 2004; Ghoroghchian, et al. 2006; Hannecart, et al. 2019; Lin, et al. 2018; Park, M., et al. 2015; Yang, et al. 2014; Zou, et al. 2015). The self-assembly behavior and critical values of f specific to PEO-*b*-PCL have extensively been studied elsewhere (Adams, D. J., et al. 2009; Du, et al. 2007; Giacomelli and Borsali 2006; Qi, et al. 2013; Zhou, et al. 2017).

For drug delivery systems, control over the particle size and shape is crucial, because they largely influence NP accumulation in various tissues upon intravenous administration, transport through physiological barriers, uptake by immune cells and clearance (Hoshyar, et al. 2016). Due to the unique self-assembly behavior of amphiphilic BCPs, the particle size and shape can be controlled by both material and process factors and it is necessary to evaluate the effects of these factors in

detail in the laboratory scale to allow further formulation-specific process optimization, scale-up and process controls.

The nanoprecipitation method, also known as the solvent displacement or anti-solvent precipitation method, is one of the most popular methods for the manufacture of polymer NPs for pharmaceutical applications (Fessi, et al. 1989; Liu, Y., et al. 2020; Martínez Rivas, et al. 2017; Miladi, et al. 2016). It is a facile and rapid method and does not require high energy input or large amounts of toxic solvents (Miladi, et al. 2016). In this method, polymer and other hydrophobic agents dissolved in a water-miscible solvent are added to an aqueous non-solvent phase under stirring, resulting in the formation of NPs by precipitation. Several studies have been performed to explain the mechanisms of particle formation by nanoprecipitation (Lavino, et al. 2017; Lebouille, J. G. J. L., et al. 2014; Lince, et al. 2008; Saad and Prud'homme 2016). Besides the polymer structure and configuration, the most critical process parameters influencing the PSD are the choice of solvent, precipitation temperature, order of addition, solvent/non-solvent ratio and ionic strength of the aqueous phase (Liu, Y., et al. 2020).

In this work, we studied how various material and process factors influence the size and morphology of PEO-*b*-PCL aggregates prepared by the nanoprecipitation method in an acetone-water system. Using a statistical approach, we evaluated the effects of f, molecular weight, mixing speed, organic phase addition rate, polymer concentration in the organic phase, water volume fraction, and precipitation temperature on the hydrodynamic diameter and polydispersity index (PDI) and examined the corresponding morphologies by cryogenic transmission electron microscopy (cryo-TEM). We created statistical models on the joint effects multiple process variables. Finally, we studied the thermal stability of the nanostructures and explored the role of kinetic control over the size and morphology of PEO-*b*-PCL NPs prepared by nanoprecipitation.

Materials and methods

Materials

Polycaprolactone-*block*-poly(ethylene oxide) methyl ether polymers (PEO-*b*-PCL) were purchased from PolymerSource, Inc. (Canada). According to the supplier, molecular weight distributions of the block copolymers were analyzed using size exclusion chromatography to determine the molecular weight of the PEO block and ^{1}H NMR to determine the final composition of the copolymer by comparing the integrated areas of PEO and PCL proton peaks. In addition, melting and glass transition temperatures of the polymers were analyzed using differential scanning calorimetry. Characteristics of the polymer samples are listed in Table 1. Volume fraction of PEO block (f_{PEO}) was calculated based on the molecular weights using literature values for solid densities of PEO and amorphous PCL at room temperature (1.15 and 1.081, respectively)(Crescenzi, et al. 1972; Rowe, et al. 2009). Acetone (≥ 99.5 %) was purchased from Sigma.

Table 1. Molecular weight data of the tested block copolymers. f_{PEO} is the PEO volume fraction calculated based on molecular weight and density of each polymer and N is the total degree of polymerization.

Product	PEO M_n (g/mol) [1]	PCL M_n (g/mol) [1]	M_w/M_n [1]	N	f_{PEO}	Short name
P5041-EOCL	2 000	1 000	1.10	54	0.65	PEO_{45}-*b*-PCL_{9}
P7170-EOCL	2 000	1 400	1.2	57	0.57	PEO_{45}-*b*-PCL_{12}
P9681-EOCL	2 000	10 000	1.19	133	0.16	PEO_{45}-*b*-PCL_{88}
P18129A-EOCL	5 000	5 000	1.18	157	0.48	PEO_{113}-*b*-PCL_{44}
P19764-EOCL	5 000	11 500	1.19	214	0.29	PEO_{113}-*b*-PCL_{101}
P19769-EOCL	5 000	25 000	1.33	332	0.16	PEO_{113}-*b*-PCL_{219}

[1] Reported by the supplier.

Experimental design

The effects of the volume fraction of water (ϕ_w), concentration of polymer in solvent (c_P), addition rate of solvent phase to the non-solvent (*A*) and rate of stirring (*S*) on the mean hydrodynamic diameter (d_H) and PDI were evaluated in this study using a Design of Experiments (DoE) approach. To allow the modelling of linear, quadratic and two-way interaction effects of each factor with a minimal amount of experimental runs, a D-optimal split-plot experimental design with three levels for each factor was created using the DoE functionality of JMP Pro 14 software (SAS). Similar approaches have been taken by several authors to optimize NP formulations (Günday Türeli, et al. 2016; Mohamadpour, et al. 2020; Tahir, et al. 2017).

The chosen process parameters and their nominal values are shown in Table 2. The defined set of 24 experimental runs (Table S1) was completed for all six polymer samples. Firstly, the full 144 runs were performed by one operator. Secondly, the runs for 5000 g/mol PEO block polymers were repeated by a different operator to gain information on reproducibility of the nanoprecipitation method and data for model validation.

Table 2. Process parameters included in the study.

Factor	Symbol	Unit of measurement	Nominal values		
Volume fraction of water	ϕ_w	-	0.43	0.62	0.71
Polymer concentration in solvent phase	c_P	mg/mL	6	13	20
Addition rate of solvent phase	A	mL/h	10	130	250
Stirring rate	S	rpm	120	460	800

Nanoprecipitation

To prepare NPs by the nanoprecipitation method, the copolymer was firstly dissolved in acetone and loaded into a plastic syringe and a steel tip was attached. The syringe was then installed onto a syringe pump (PHD2000, Harvard Apparatus), a piece of low-density polyethylene tubing was attached and the solution was injected into 1.2 mL of Milli-Q water in a 4 mL glass vial under magnetic stirring at a controlled rate. During injection, the end of the tubing was immersed below the surface of water, close to the spinning magnet (see Scheme 1).

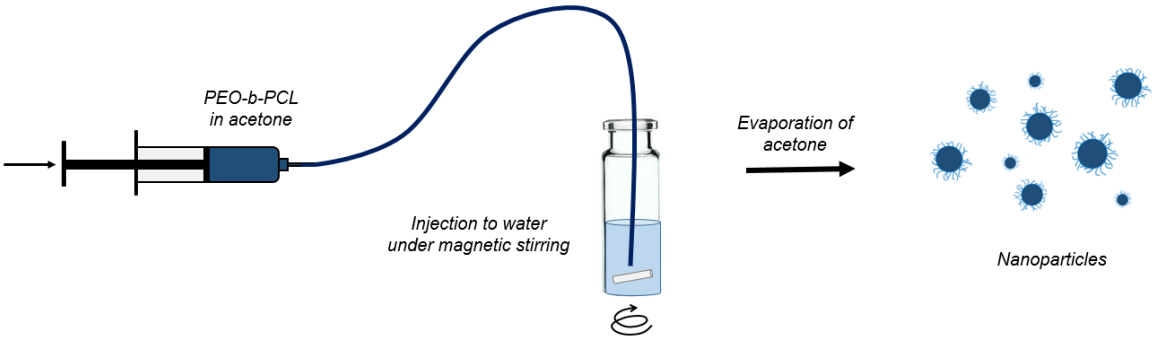

Scheme 1. Preparation of PEO-b-PCL nanoparticles by the nanoprecipitation method.

The resulting dispersions were stirred at room temperature for 20-24 h in open vials to allow evaporation of acetone. All samples were prepared at room temperature, unless otherwise specified, stored at room temperature in closed vials, and dynamic light scattering (DLS) analysis was performed within three days from preparation. Acetone was chosen as the organic solvent due to its miscibility with water, ability dissolve both polymer blocks, low toxicity (ICH Q3C Class 3) (EMA 2019), and facile removal by evaporation.

Dynamic Light Scattering

Particle size distributions were analyzed by DLS using Zetasizer Nano ZS (Malvern) at a scattering angle of 173 °. Attenuator setting, measurement position and the number of runs per measurement were chosen automatically by the instrument, compensating for variations in scattering signal strength arising from differences in particle size and concentration. The Zetasizer software (v. 7.11) calculates mean hydrodynamic diameter and PDI based on particle diffusivity. No pre-treatments (*e.g.*, filtering and extrusion) were performed prior to DLS measurement. All measurements were performed in triplicates.

Cryo-TEM analysis

Selected samples were imaged by cryo-TEM. No pre-treatments (*e.g.*, filtering and extrusion) were performed for the samples. A 5 µL drop of nanoparticle dispersion (2 mg/mL) was applied onto plasma-treated lacey carbon coated copper grids (Electron Microscopy Sciences). The drop was blotted with filter paper and plunged into liquid ethane (–170 °C) using an automatic plunge freezer (EM GP2, Leica) and stored in liquid nitrogen. The samples were inspected using JEM-3200FSC (JEOL) microscope at 300 kV acceleration voltage and images were acquired using Digital Micrograph software (Gatan).

Results and discussion

Effects of polymer configuration on size and morphology

To study the effects of polymer molecular weight and block lengths, nanoparticles were prepared by the nanoprecipitation method, as described above, and a general characterization by DLS and cryo-TEM was performed. The process parameters used in the preparation of these NP samples are listed in Table S2. Representative micrographs of the formed nanostructures are shown in Figure 2, including DLS size distribution histograms based on scattering intensity. A summary of the observed nanoscale morphologies is shown in Table 3.

Nanostructures of various shapes were observed in the studied samples. For PEO_{45}-*b*-PCL_{9} ($f_{PEO} = 0.65$) and PEO_{45}-*b*-PCL_{12} ($f_{PEO} = 0.57$), the dominant morphology was long thread-like micelles with a diameter of 13 ± 2 nm and 13 ± 3 nm, respectively, and length up to several microns (Figure 2 a-b). In addition, a small population of spheres with an average diameter of 12 nm was observed in both samples. For all other samples, the dominant nanoscale morphology was spherical. As measured from the micrographs, the diameter of the spheres was 26 ± 9 nm for PEO_{45}-*b*-PCL_{88}, 25 ± 9 for PEO_{113}-*b*-PCL_{44}, and 17 ± 7 nm for PEO_{113}-*b*-PCL_{101}. Besides spheres, PEO_{113}-*b*-PCL_{44}

samples contained also notable amounts of worm-like micelles. PEO_{45}-*b*-PCL_{88} samples also contained small amounts of sheet-like and lamellar structures.

The morphology assumed by PEO-b-PCL has been shown to be highly dependent on both material and process factors and the overlapping of multiple different morphologies has been commonly reported even for narrow molecular weight distribution polymers. For example, Adams *et al.* studied vesicle formation induced by slow sequential addition of water into a solution of PEO-b-PCL in tetrahydrofuran (THF) and mapped the resulting aqueous equilibrium morphologies as a function of f_{PEO}. They showed that vesicles were the dominant morphology at $f_{PEO} \approx 0.15 - 0.23$, whereas mainly worm-like micelles were present at $f_{PEO} \approx 0.25 - 0.32$ and spherical micelles at $f_{PEO} \geq 0.3$, with a partial overlap of different morphologies (Adams, D. J., et al. 2009). In another study, polymersomes were successfully generated from samples with f_{PEO} ranging from 0.14 to 0.27 and PEO molecular weight between 750 and 3800 g/mol using an aqueous hydration and extrusion method (Qi, et al. 2013).

In the present work, no vesicles were observed for any of the samples, even though polymers similar to PEO_{45}-*b*-PCL_{88} ($f_{PEO} = 0.16$) have been used to form vesicles, as described above, using different methods. Similar findings on the inability of the room-temperature solvent displacement methods to produce PEO-b-PCL polymersomes can be found in the literature (Sui, et al. 2015; Zhou, et al. 2017). Sui *et al*. demonstrated that PEO-b-PCL with f_{PEO} ranging from 0.17 to 0.32 formed spherical micelles by solvent displacement method using a THF-water system, whereas a mixture of spherical micelles and polymersomes was obtained by thin film hydration and direct hydration methods (Sui, et al. 2015). In another study, Zhou *et al*., successfully prepared PEO-b-PCL vesicles by solvent displacement using a THF-water system at elevated temperatures (> 50 °C), whereas an acetone-water system was unable to produce vesicles regardless of precipitation temperature (Zhou, et al. 2017).

The formation of high aspect ratio thread-like morphology of PEO-*b*-PCL with $f_{PEO} \geq 0.5$ precipitated from acetone (Figure 2a-b) in the present work is in agreement with the work of Giacomelli and Borsali (Giacomelli and Borsali 2006). In their work, PEO-b-PCL with $f_{PEO} = 0.50 - 0.58$ formed spherical micelles when dialyzed from THF or dimethylformamide (DMF), but resulted in long thread-like micelles when acetone was used as the starting solvent.

The formation of vesicles is known to occur through a sequence of morphologies: individual polymer chains first aggregate to spherical micelles, which then transform to rods and finally vesicles as the water concentration is increased. This sequence can be explained as an attempt to minimize the free energy associated with the interface between the PCL core and the surrounding solvent by aggregate fusion and reorganization into structures of reduced curvature to minimize the interfacial area (Choucair and Eisenberg 2003). Besides interfacial energy, other important driving forces for

these transitions include the entropic process of stretching of the core-forming block and possible electrostatic repulsion between corona-forming blocks (Choucair and Eisenberg 2003). In this work, a methoxy-terminated PEO was used as the corona-forming block, which is charge-neutral, hence electrostatic repulsion does not play a role here.

Compared to THF, acetone is a poorer solvent for PCL (Bordes, et al. 2010). Using a poorer solvent will reduce the degree of swelling of the core and the degree of PCL chain stretching. Diminished core chain stretching reduces the driving force for rearrangement into cylinders and vesicles and results in a kinetically trapped metastable morphology, a phenomenon that has been described in detail for polystyrene-block-poly(acrylic acid) polymers (Choucair and Eisenberg 2003). This can explain the appearance of thread-like micelles at $f_{PEO} \geq 0.5$ as well as the lack of vesicles at $f_{PEO} = 0.16$ when using this water-acetone system.

In addition to the nanostructures shown in Figure 4 and Table 3, all of the studied samples contained small amounts of larger objects of various shapes in the micron-scale. This was expected as the samples were not filtered or extruded. Such pre-treatments were omitted to obtain samples that are representative of the true results of the nanoprecipitation process. The observed large structures may result from contamination, impurities, agglomeration of particles or undissolved polymer.

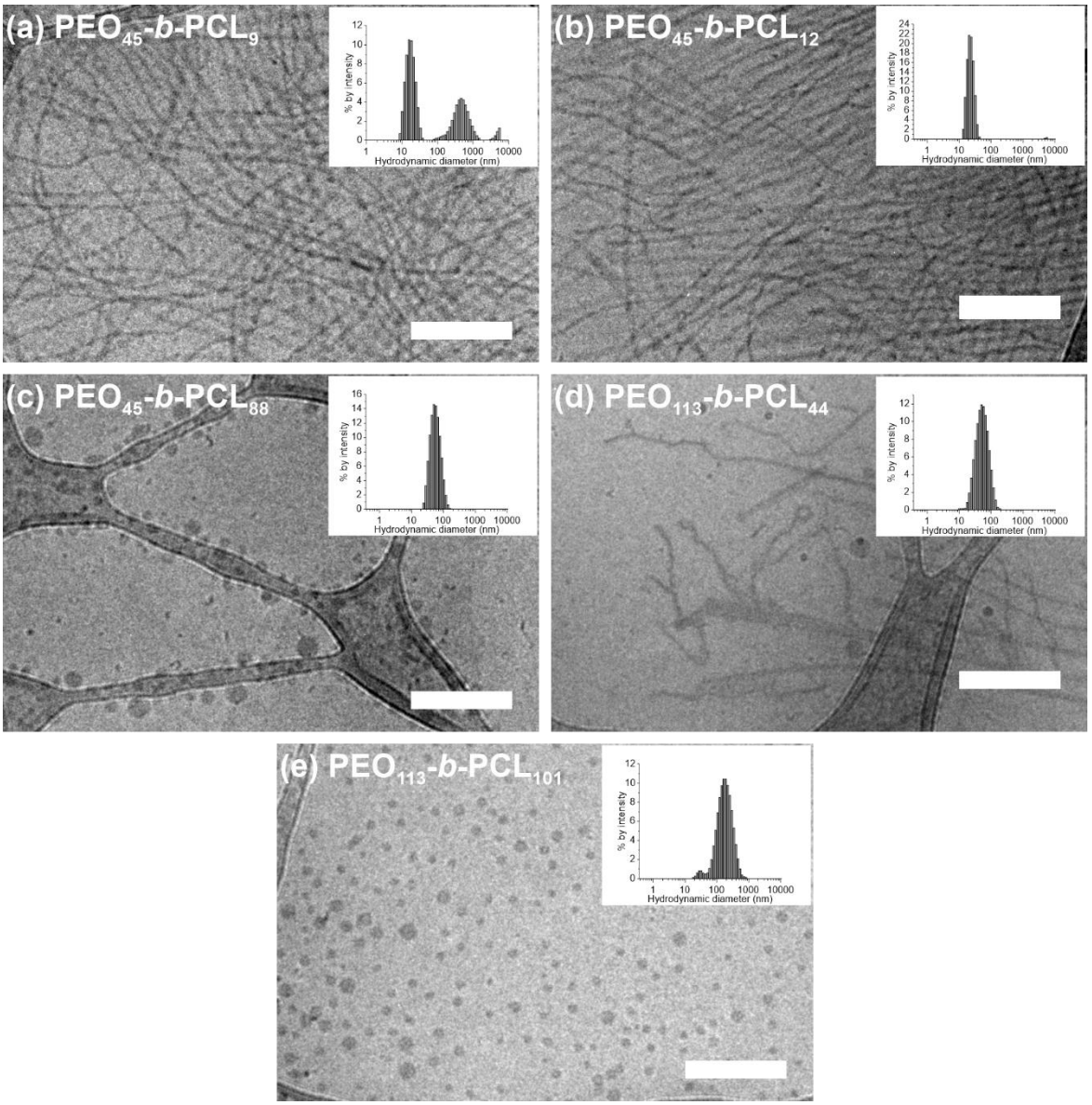

Figure 2. Representative micrographs of nanostructures formed from PEO-b-PCL with different block lengths. Size distributions obtained by dynamic light scattering are presented in inserts. Nanoprecipitation was performed at room temperature. Scale bars are 200 nm. Dark thick objects are the carbon film of the cryo-TEM grid.

Table 3. Summary of the observed nanoscale morphologies, where S = solid spheres, W = worm-like or fiber-like structures, L = lamellar or sheet-like structures, V = vesicles. Multiple morphologies are listed in order of abundance.

Polymer	N	f_{PEO}	Nanoscale morphology		
			Precipitation at R.T.	Precipitation at 65 °C	Precipitation at R.T. + heat-treatment
PEO_{45}-*b*-PCL_{9}	54	0.65	W, (S)	W, S	--
PEO_{45}-*b*-PCL_{12}	57	0.57	W, S	W, S	--
PEO_{45}-*b*-PCL_{88}	133	0.16	S, L	S, L, V	--
PEO_{113}-*b*-PCL_{44}	157	0.48	S, W	S, (W)	S, (W)
PEO_{113}-*b*-PCL_{101}	214	0.29	S	S	S, (V)

Statistical overview on the effect or process factors on PSD

Firstly, a simple linear correlation analysis was performed for the obtained DLS data. PEO_{45}-*b*-PCL_{9} ($f_{PEO} = 0.65$) and PEO_{45}-*b*-PCL_{12} ($f_{PEO} = 0.57$) samples were excluded from all statistical analyses due to a non-spherical morphology. Linear correlations between the variables were evaluated by calculating Pearson correlation coefficients (Table S3), also presented in the form of heat maps in Figure 3. The numerical data (Table S3) shows that d_H and PDI correlated significantly ($p \leq 0.05$) only with *N*, f_{PEO}, ϕ_w and with each other. The effects of *N*, f_{PEO} and ϕ_w are shown in Figure 4 in the form of dot plots. The data shown in Figures 3-4 and Table S3 contain all the acquired d_H values, including those associated with very high PDI and multimodal PSD. As the PDI values approach unity and multiple peaks appear, it becomes meaningless to use d_H to describe the PSD. Despite these limitations, some conclusions can be made based on the obtained data.

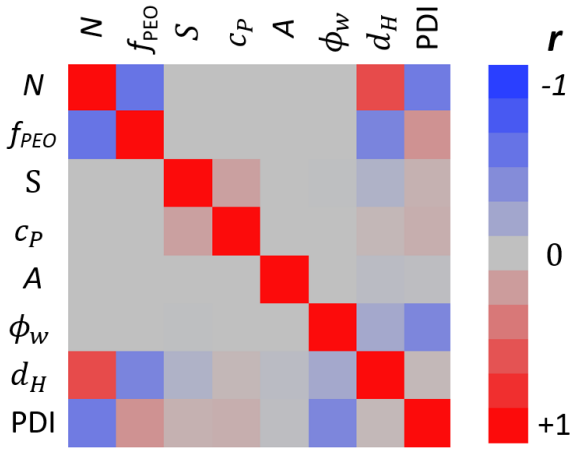

Figure 3. Linear correlations of variables visualized by heat maps, where N = polymerization degree, f_{PEO} = PEO volume fraction, S = stirring rate, c_P = concentration of polymer in organic phase, A = addition rate of organic to water, ϕ_W = water volume fraction, d_H = mean hydrodynamic diameter

and PDI obtained by DLS. Data from polymers with a non-spherical dominant morphology have been excluded from the analyses. For the colored figure, the reader is referred to the web version of this article.

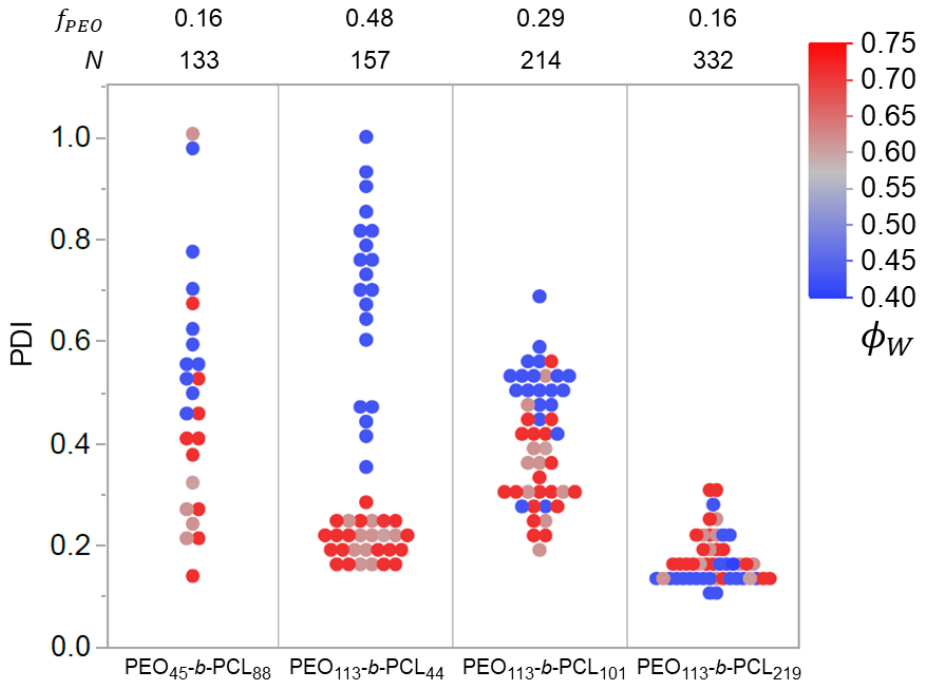

Figure 4. Dot plot of polydispersity index (PDI) values as a function of PEO block volume fraction (f_{PEO}), total degree of polymerization (N) and water volume fraction (ϕ_w). For the colored figure, the reader is referred to the web version of this article.

Firstly, the degree of polymerization (or molecular weight, MW) had a negative correlation with PDI, indicating that higher MW polymers resulted in a narrower PSD. This can be partly explained by the higher degree of supersaturation achieved for high MW polymers due to their lower solubility. The nanoprecipitation method is based on rapid reduction of solvent quality, leading to the precipitation of NPs. High supersaturation favors nucleation over particle growth, leading to small particles with a narrow PSD (Johnson and Prud'homme 2003).

Another explanation for high PDI values at low MW is that a wider range of morphologies is obtained with lower molecular weight polymers, as can be seen from Figure 2 and Table 3. This explanation is supported by the findings of Du *et al*., who showed by TEM analysis that PEO-*b*-PCL with higher PEO block lengths (5000 g/mol) assumed a spherical morphology through a wide range of PCL block lengths, whereas polymers with shorter PEO blocks (2000 g/mol) showed more diverse

morphologies (spheres, worm-like micelles, and lamellae) over the PCL block lengths studied (Du, et al. 2007).

Secondly, for PEO_{113}-*b*-PCL_{44} and PEO_{113}-*b*-PCL_{101}, significantly higher PDI values were obtained at low ϕ_W and this effect was more pronounced for PEO_{113}-*b*-PCL_{44}. This can be explained by partial solubility of the hydrophobic block in the dispersing medium when the PCL block length and ϕ_W are both small, resulting in low supersaturation and possible agglomeration of NPs. The effect of ϕ_W on the PSD and morphology is explored in more detail later in this work.

Selection of data for statistical modelling

A set of criteria was put in place to choose what data to include for a more detailed statistical analysis of process parameter effects on d_H and PDI. Using d_H to describe the PSD is meaningful only when the particles are spherical, their PSD is unimodal and PDI is relatively low. Therefore, only polymers for which unimodal PSDs were typically obtained, were included in the study. Only PEO_{113}-*b*-PCL_{219} and PEO_{45}-*b*-PCL_{88}, polymers with $f_{PEO} = 0.16$, fulfilled this criterion. Additionally, only data points corresponding to PDI < 0.5 were included in statistical models.

Model of process parameter effects for PEO_{113}-b-PCL_{219}

The lowest PDI values were obtained with the highest molecular weight polymer, PEO_{113}-*b*-PCL_{219}. Therefore, the effects of process parameters on PDI and d_H were first evaluated by creating a model exclusively for this polymer. Both linear regression models and quadratic mixed models were created by standard least squares method using the Fit Model function of JMP Pro 14 software. Model coefficients are available in Tables S4-S6. Qualities of fit of each model are summarized in Table 4.

A linear regression model for PEO_{113}-*b*-PCL_{219} using the four process variables could predict d_H reasonably well ($R^2_{adj} = 0.83$, $p \ll 0.05$), while a linear model for PDI was not able to explain the variance ($R^2_{adj} = 0.41$, $p = 0.74$). Fixed effect tests of the d_H model showed that the effects of S, c_P and ϕ_w were statistically significant ($p < 0.05$), whereas the effect of addition rate (A) was not significant ($p = 0.31$). The directions and magnitudes of each effect are shown as leverage plots in Figure S4.

According to the linear model, an increase in the stirring rate and water fraction decreased the average particle size, which can be explained by increased local supersaturation, leading to nucleation-favoring conditions. The model also implies that particle size was increased by an increase in polymer concentration in solvent phase. These qualitative findings are well supported by

other literature reports (Johnson and Prud'homme 2003; Lebouille, J. G. J. L., et al. 2014). Particle size was not strongly affected by changes in addition rate within the range studied here (10 to 250 mL/h).

Quadratic models containing all squared effects and two-way interactions (a total of 14 effects), resulted in $R^2_{adj} = 0.93$ and 0.37 for d_H and PDI, respectively. To simplify the quadratic models, effects were manually excluded one-by-one to maximize the coefficient of determination, while minimizing the amount of remaining effects and the root-mean-square error of prediction (RMSE). The effects c_P^2, S^2, ϕ_W^2, $c_P A$ and $c_P \phi_w$ were removed from the model of d_H, resulting in a model with nine effects and $R^2_{adj} = 0.92$. Similarly, all squared interactions were removed from the PDI model, which greatly improved model quality in terms of adjusted R^2 and RMSE (See Table 4).

The simplified quadratic models for PEO_{113}-*b*-PCL_{219} are visualized in Figure 5 using response surface plots. The effects of ϕ_W, S and c_P on d_H were very similar to the linear model. The effect of addition rate was small in magnitude. Looking at the standardized model coefficients (Table S6) it can be seen that an increase in the terms of ϕ_W, S , A and $c_P S$ was associated with a decrease in particle size, whereas increasing the c_P, A^2, $\phi_W S$, $\phi_W A$ and SA terms was associated with an increase in particle size in this particular data set.

Table 4. Qualities of fit of the statistical models of process parameter effects created for PEO_{113}-b-PCL_{219}. RMSE = root-mean-square error of prediction and R^2_{adj} is the adjusted coefficient of determination.

Response	Model type	Number of effects	R^2	R^2_{adj}	RMSE
d_H	Linear	4	0.86	0.83	9.99
	Quadratic, full	14	0.97	0.93	7.26
	Quadratic, simplified	9	0.96	0.94	6.69
PDI	Linear	4	0.52	0.41	0.036
	Quadratic, full	14	0.75	0.37	0.031
	Quadratic, simplified	10	0.76	0.57	0.028

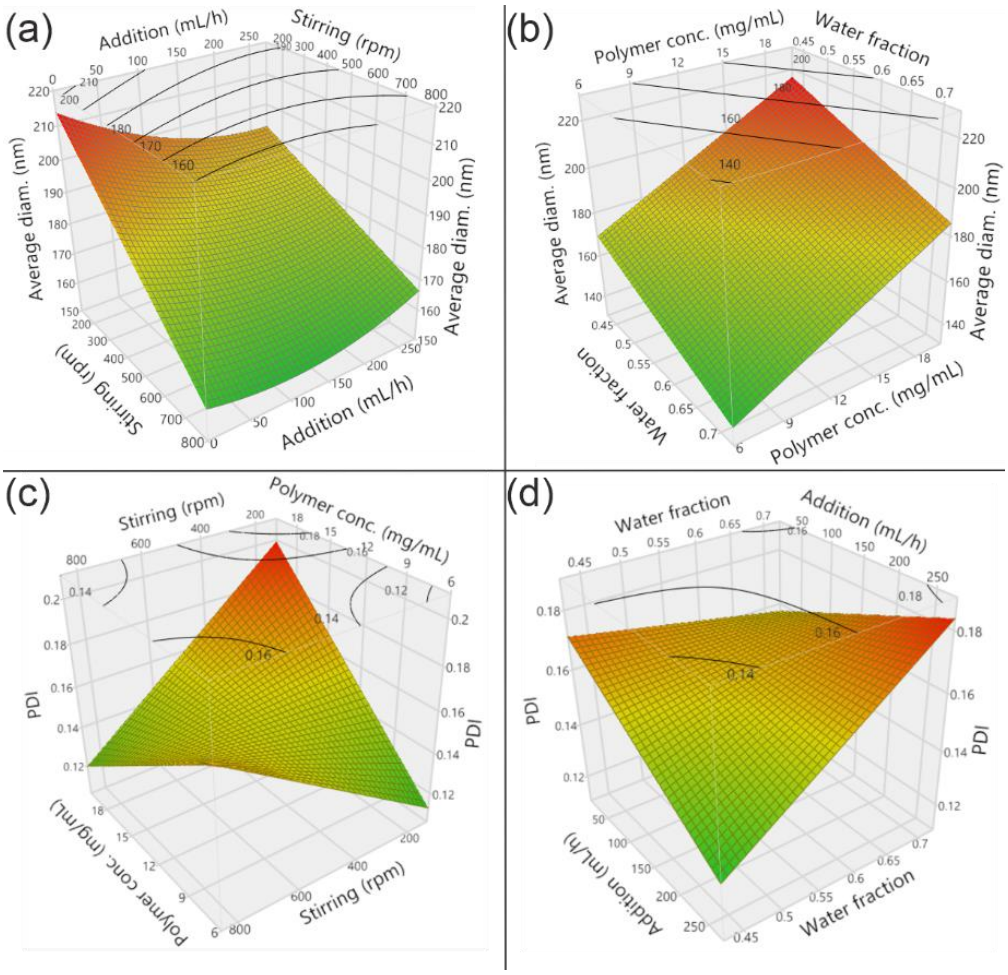

Figure 5. Response surface plots of the simplified quadratic model for PEO_{113}-b-PCL_{219} on the effect of nanoprecipitation parameters on mean hydrodynamic diameter (a-b) and PDI (c-d).

Reproducibility and the operator effect

To evaluate the reproducibility of the nanoprecipitation method and to provide data for model validation, the experimental runs for 5000 g/mol PEO block polymers were repeated by a second operator, yielding a second data set. Both operators performed the experimental runs with identical protocols, equipment, parameters and instructions. Figure 7 shows a scatterplot of d_H values of the two data sets plotted against the prediction of the simplified quadratic model, which is shown as a straight line. The model was created based on the first data set. It can be seen that both data sets clearly correlated with the model. However, the fit was poorer for the second data set. There was visible systematic error as the second set contained, on average, higher values than the first.

Reproducibility of the basic nanoprecipitation method is limited due to insufficient control over mixing conditions. In this work, the method was modified to specifically reduce the variation in mixing conditions by injecting the polymer solution via a tube at a controlled rate. In spite of this modification, systematically higher d_H values were observed with the second operator. Besides person-to-person

differences in sample preparation, another possible explanation for this variance is the partial hydrolysis of PCL during storage, in either the dissolved or the solid state. Solid polymers were stored in dry, closed vials in a refrigerator for several months between the two data sets. Polymer solutions were stored in tightly sealed flasks at room temperature and storage time varied from days to weeks. However, hydrolysis of PCL is expected to reduce the molecular weight, and thus, particle size, which is opposite to the general trend seen in Figure 6. Therefore, it is unlikely that the differences between data sets are caused simply by polymer hydrolysis. Yet another possible source of variance is the lack of filtering of solutions prior to nanoprecipitation and samples prior to analysis, which may result in contamination that can affect the size distribution.

In light of the possible confounding effects listed above and considering that only two operators were included in these tests, no strong conclusions can be made on the operator effect. Nevertheless, the results underline the challenges in reproducibility of this method and the need for strict control of both material and process factors for obtaining a homogeneous end product.

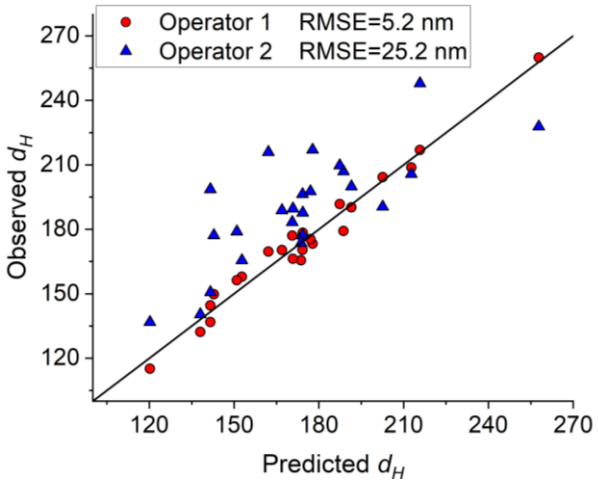

Figure 6. Observed *vs*. predicted values plot for the simplified quadratic model for average hydrodynamic diameter. Observed d_H values of the first data set (operator 1, red spheres) and second data set (operator 2, blue triangles) are plotted against the prediction of the model, which has been created based on the first data set. Straight line represents a perfect fit.

Combined effects of molecular weight and process factors

To include the effect of molecular weight in the models, new models were created based on data from both f_{PEO} = 0.16 polymers (PEO_{45}-*b*-PCL_{88} and PEO_{113}-b-PCL_{219}) using the same method as above. Data sets from the both operators were included, but operator effect was not included as an independent variable. Data points with PDI > 0.6 were excluded (n = 6). The full quadratic models, containing 19 effects each, were able to explain 92% of the variance in d_H (R^2_{adj} = 0.92, RMSE = 14.6 nm) and 79% of the variance in PDI (R^2_{adj} = 0.79, RMSE = 0.059). The models were simplified by manually removing the effects with minor contributions and recalculated.

The simplified models, containing eight effects for d_H and five effects for PDI, were able to explain 90% (R^2_{adj} = 0.90, RMSE = 14.5 nm) and 80% (R^2_{adj} = 0.80, RMSE = 0.060) of the variances of d_H and PDI, respectively. Fixed effect tests showed that all the included effects were statistically significant ($p < 0.05$). The coefficients of both models are listed in Table S7. Response surface plots based on the simplified model are presented in Figure 7. According to the standardized model coefficients, the strongest predictor for particle size is the molecular weight and other important variables are the polymer concentration, stirring rate and water fraction. Once again, addition rate did not strongly affect the responses.

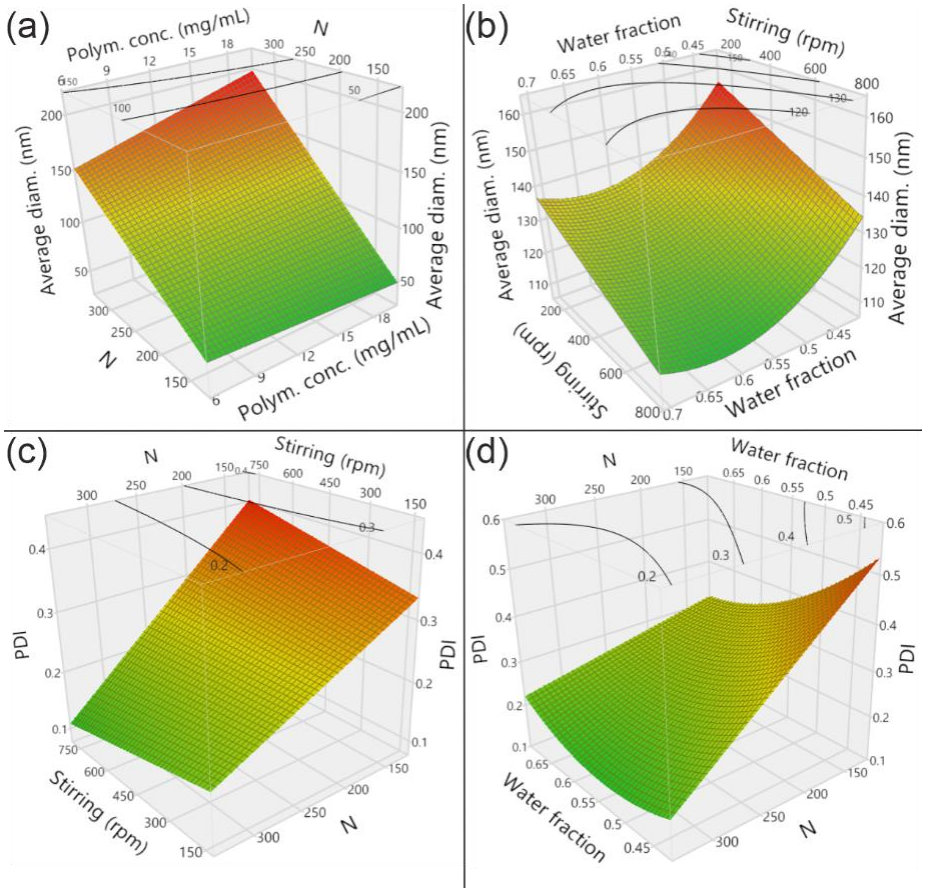

Figure 7. Response surface plots of simplified quadratic models for hydrodynamic diameter (a-b) and PDI (c-d) for polymers with PEO volume fraction of 0.16. This model includes the data from both operators.

Effect of water volume fraction

As previously discussed, PDI was found to correlate with water volume fraction, ϕ_w, especially strongly for PEO_{113}-*b*-PCL_{44} and PEO_{113}-*b*-PCL_{101}. To study this dependency in more detail, additional experiments were conducted with ϕ_w ranging from 0.40 to 0.875 (see Table S2 for details).

The obtained values for d_H and PDI are plotted as a function of ϕ_w in Figure 8. Representative low-magnification micrographs and DLS data from selected samples are shown in Figure S1.

According to Lince *et al.*, the solubility of PCL (14 000 g/mol) in acetone-water mixtures drops significantly at water mole fractions of 0.4 to 0.5 (Lince, et al. 2008), which correspond to ϕ_w of 0.14 to 0.20. This means that to obtain a high level of supersaturation, ϕ_w far in excess of 0.20 should be used. Our data of PEO_{113}-*b*-PCL_{101} in Figure 8 shows that for this micelle-forming polymer, nanoprecipitation with ϕ_w as low as 0.4 did not cause widening of the PSD. However, for PEO_{113}-*b*-PCL_{44} with a shorter PCL block, very wide PSDs were obtained below $\phi_w = 0.5$. This is explained by the higher solubility of a shorter PCL block in the dispersing medium: a shorter PCL block requires a stronger reduction in solvent quality to achieve a high enough supersaturation to obtain a narrow PSD. Additionally, the data shows that further increase of ϕ_w above 0.55 did not reduce PDI or average hydrodynamic size for these polymers, showing that this parameter is a poor choice for fine-tuning of particle size for these polymers.

According to the cryo-TEM analyses, a population of large structures appeared for PEO_{113}-b-PCL_{44} at low ϕ_W (Figure S1a), which explains the associated high PDI values. These flat objects have an oval cross-section resembling a rice-grain and range from 1 to 8 µm in length and they were abundant in PEO_{113}-b-PCL_{44}, but scarce in the PEO_{113}-b-PCL_{101} samples. Closer investigation of these oval-shaped structures suggests that they consist of agglomerated worm-like micelles (Figure S2) and they seem to form in large numbers when ϕ_w is reduced below ≈ 0.5. For the micelle-forming PEO_{113}-*b*-PCL_{101} ($f_{PEO} = 0.29$), size and PDI are largely unaffected by changes in water volume fraction within the studied range, and some larger agglomerates were found regardless of ϕ_w (Figure S1 d-f). Dominant nanoscale morphologies did not change as a function of ϕ_W for either of the samples tested.

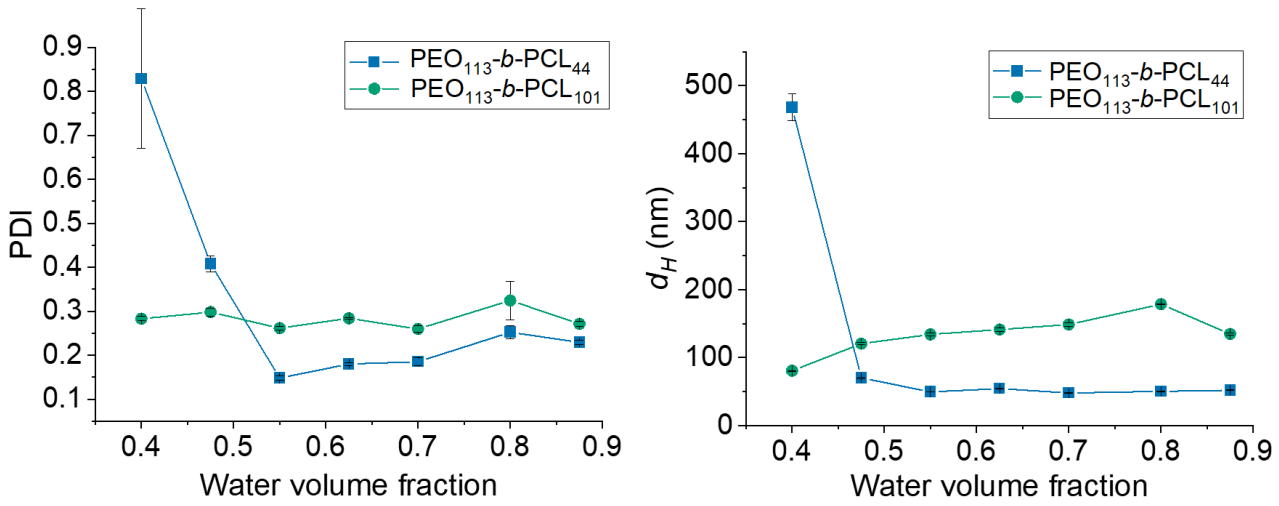

Figure 8. Polydispersity index (PDI) and mean hydrodynamic diameter (d_H) as a function of water volume fraction. Error bars show ± standard deviation (SD) of three repeat measurements of a single sample. Lines connecting the data points have been added only for visual clarity.

Effect of precipitation temperature and evaluation of stability above melting point

As discussed above, kinetic trapping of polymer chains into non-equilibrium morphologies plays a role in BCP nanoprecipitation. This was further evidenced in the present work by the fact that no vesicles were formed from PEO_{45}-*b*-PCL_{88} ($f_{PEO} = 0.16$) by simple nanoprecipitation. The PCL NP core can crystallize (Du, et al. 2007; Rajagopal, et al. 2010), which further increases the kinetic barrier for chain reorganization into vesicles. Therefore, we were interested to see whether maintaining temperature above the melting point of PCL ($T_m \approx 55$ °C) during nanoprecipitation, effectively preventing crystallization, could affect the morphology (Zhou, et al. 2017).

In this experiment, nanoprecipitation was performed as previously, but in a heated water bath. The temperature of the water phase was adjusted to 65 °C ± 1 °C prior to injection of the organic phase (see Table S2 for parameters). After injection, acetone quickly evaporated as the temperature was above its boiling point. The temperature of the mixture was not monitored after injection. After solvent evaporation, the samples were analyzed by DLS and imaged by cryo-TEM, as previously described. The obtained d_H and PDI values are shown in Figure 9 and representative micrographs are shown in Figure 10a-e. Light scattering data is presented only for the polymers that formed spherical particles.

It can be seen that performing nanoprecipitation at elevated temperatures caused an increase in PDI and d_H, with the exception of the micelle-forming polymer PEO_{113}-*b*-PCL_{101}, for which no significant change in particle size was observed as a function of temperature. Size increase was the strongest for PEO_{45}-*b*-PCL_{88}. Cryo-TEM analyses showed that the increase in precipitation temperature caused only minor changes in morphology. Dominant morphologies for each polymer remained identical to the corresponding samples at room temperature. In the high-temperature sample PEO_{45}-*b*-PCL_{88}, a small population of vesicles appeared in addition to solid spherical particles (Figure 10c), even though no vesicles were observed in the room temperature sample of this polymer (Figure 2c). In addition, lamellar or ladder-like structures were observed, examples of which can be seen in Figure S3.

Zhou *et al*. developed a temperature-assisted nanoprecipitation method for the production of PEO-*b*-PCL vesicles. They showed that when THF was used as the organic solvent, increasing the precipitation temperature above 50 °C allowed the formation of vesicles from polymer with $f_{PEO} = 0.12$, whereas precipitation at room temperature was unable to produce vesicles. They reported that precipitation from acetone was unable to produce vesicles from this polymer even at elevated temperatures (Zhou et al. 2017). Our data also shows that a small population of vesicles did form from polymer with $f_{PEO} = 0.16$ at 65 °C, when using acetone as the organic solvent.

In another experiment, we wanted to study whether heating the already prepared NPs could change their morphology, when heated above the melting point of PCL. Aliquots of analyzed room-temperature precipitated samples of PEO_{113}-*b*-PCL_{101} and PEO_{113}-*b*-PCL_{44} were placed in a 65 °C ± 1 °C water bath with moderate magnetic stirring for 30 min. After equilibrating to room temperature, the heat-treated samples were re-analyzed by DLS and cryo-TEM. The obtained d_H and PDI values are shown in Figure 9, and the representative micrographs are shown in Figure 10f-g. The data shows that heat treatment did not have a strong effect on hydrodynamic size. A small increase of PDI was seen with PEO_{113}-*b*-PCL_{44}. Cryo-TEM investigation showed a very small population of vesicles in the sample of PEO_{113}-*b*-PCL_{101} after heat-treatment, whereas no vesicles were observed in the same sample prior to the heat treatment (Figure 2e).

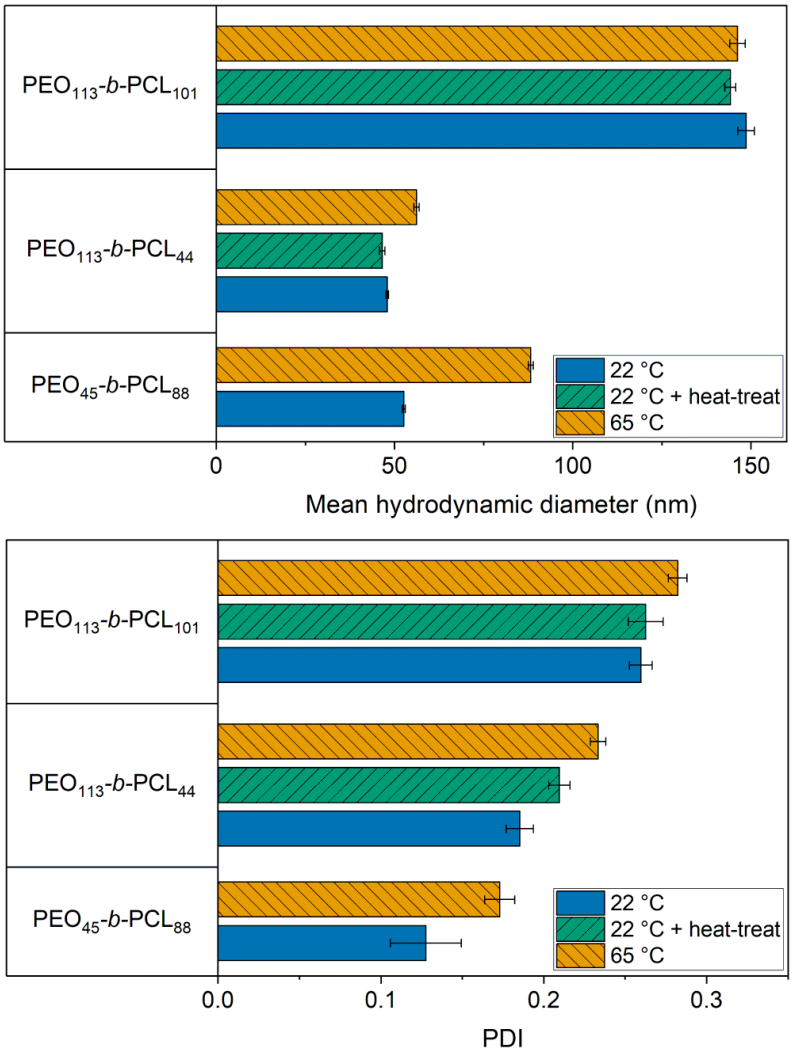

Figure 9. PDI and mean hydrodynamic diameter of samples precipitated at room temperature (≈ 22 °C) and at 65 °C, as well as room-temperature samples heat-treated at 65 °C for 30 min. All samples were analyzed at room temperature. Error bars show ±SD of three repeat measurements of a single sample.

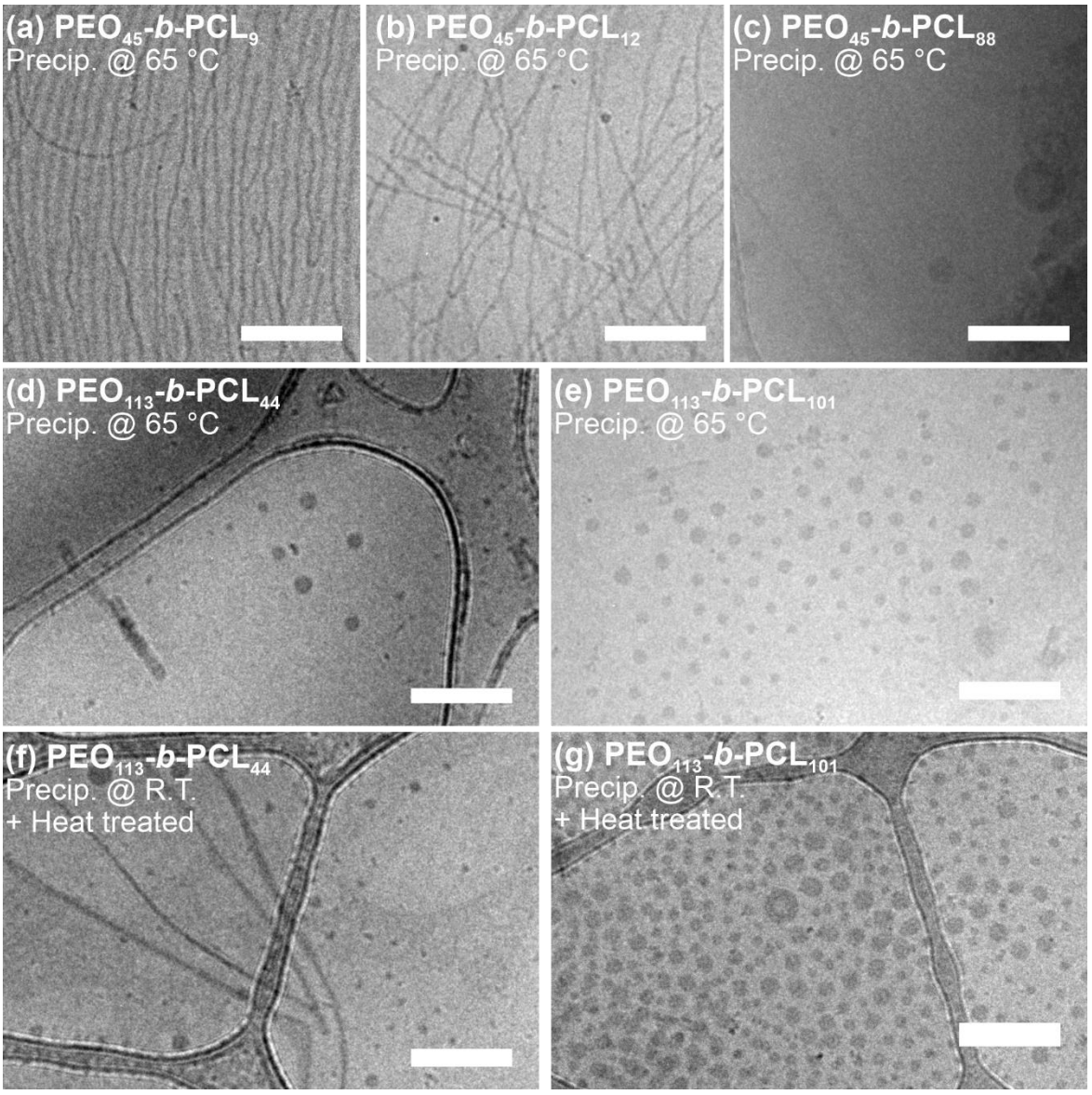

Figure 10. Representative micrographs of the formed nanostructures when nanoprecipitation was performed at 65 °C (a-e) or when the nanoprecipitation was performed at room temperature and the samples were heat-treated (30 min, 65 °C) after solvent evaporation (f-g). Scale bars are 200 nm.

In contrast to lipids or low-molecular weight surfactants, the ability of polymer chains to re-arrange after the initial precipitation step is limited. Due to this lack of molecular mobility, the choice of manufacturing method and parameters is crucial in obtaining the desired morphology. Our observations underline that the morphology of BCP NPs is dictated not only by polymer configuration, but largely also by the manufacturing process. Block copolymers that have a vesicular aqueous equilibrium morphology can be used to prepare solid NPs by the kinetic control enabled through rapid quenching by nanoprecipitation. Formulating solid NPs from BCPs with long hydrophobic blocks, such as the f_{PEO} = 0.16 polymers used here, can be beneficial in terms of

achieving a higher loading capacity of hydrophobic drugs per NP (Lim Soo, et al. 2005; Shi, et al. 2005).

Conclusions

We have evaluated the effects of nanoprecipitation process parameters on the PSD and morphology of PEO-*b*-PCL aggregates using a statistical modelling approach. The most important variables affecting the PSD were identified and visualized and statistical models were created capable of explaining up to 94% in the variance of d_H. In addition, the effects of water volume fraction and precipitation temperature were examined in detail and we found that increasing the precipitation temperature could facilitate the formation of vesicles. The data highlights that achieving a reproducible production of nanoparticles requires a very strict control over both material and process factors. Overall, the findings of this work can enable the rational choice of parameters for any formulation-specific optimization studies and we hope that this work inspires more mechanistic studies on preparation methods of colloidal drug delivery systems from block copolymers.

Conflict of Interests

V. Balasubramanian is an employee at Bayer Oy (Finland). The other authors declare no conflict of interest.

Acknowledgements

Bayer Oy (Finland) is acknowledged for financial support.

References

Adams, D.J., Kitchen, C., Adams, S., Furzeland, S., Atkins, D., Schuetz, P., Fernyhough, C.M., Tzokova, N., Ryan, A.J., Butler, M.F., 2009. On the mechanism of formation of vesicles from poly(ethylene oxide)-block-poly(caprolactone) copolymers. Soft Matter 5, 3086-3096.

Adams, M.L., Lavasanifar, A., Kwon, G.S., 2003. Amphiphilic block copolymers for drug delivery. J. Pharm. Sci. 92, 1343-1355.

Ahmed, F., Discher, D.E., 2004. Self-porating polymersomes of PEG–PLA and PEG–PCL: hydrolysis-triggered controlled release vesicles. J. Control. Release 96, 37-53.

Ali, R., Farah, A., Binkhathlan, Z., 2017. Development and characterization of methoxy poly (ethylene oxide)-block-poly(epsilon-caprolactone) (PEO-b-PCL) micelles as vehicles for the solubilization and delivery of tacrolimus. Saudi Pharm. J. 25, 258-265.

Allen, C., Yu, Y., Maysinger, D., Eisenberg, A., 1998. Polycaprolactone-b-poly(ethylene Oxide) Block Copolymer Micelles as a Novel Drug Delivery Vehicle for Neurotrophic Agents FK506 and L-685,818. Bioconjugate Chem. 9, 564-572.

Anselmo, A.C., Mitragotri, S., 2019. Nanoparticles in the clinic: An update. Bioeng Transl Med. 4, e10143.

Bobo, D., Robinson, K.J., Islam, J., Thurecht, K.J., Corrie, S.R., 2016. Nanoparticle-Based Medicines: A Review of FDA-Approved Materials and Clinical Trials to Date. Pharm. Res. 33, 2373-2387.

Bordes, C., Fréville, V., Ruffin, E., Marote, P., Gauvrit, J.Y., Briançon, S., Lantéri, P., 2010. Determination of poly(ε-caprolactone) solubility parameters: Application to solvent substitution in a microencapsulation process. Int. J. Pharm. 383, 236-243.

Choucair, A., Eisenberg, A., 2003. Control of amphiphilic block copolymer morphologies using solution conditions. Eur. Phys. J. E 10, 37-44.

Crescenzi, V., Manzini, G., Calzolari, G., Borri, C., 1972. Thermodynamics of fusion of poly-β-propiolactone and poly-ε-caprolactone. comparative analysis of the melting of aliphatic polylactone and polyester chains. Eur. Polym. J. 8, 449-463.

Deng, H., Liu, J., Zhao, X., Zhang, Y., Liu, J., Xu, S., Deng, L., Dong, A., Zhang, J., 2014. PEG-b-PCL Copolymer Micelles with the Ability of pH-Controlled Negative-to-Positive Charge Reversal for Intracellular Delivery of Doxorubicin. Biomacromolecules 15, 4281-4292.

Discher, D.E., Ahmed, F., 2006. POLYMERSOMES. Annu. Rev. Biomed. Eng. 8, 323-341.

Dong, P., Wang, X., Gu, Y., Wang, Y., Wang, Y., Gong, C., Luo, F., Guo, G., Zhao, X., Wei, Y., Qian, Z., 2010. Self-assembled biodegradable micelles based on star-shaped PCL-b-PEG copolymers for chemotherapeutic drug delivery. Colloids Surf., A 358, 128-134.

Du, Z., Xu, J., Fan, Z., 2007. Micellar morphologies of poly(epsilon-caprolactone)-b-poly(ethylene oxide) block copolymers in water with a crystalline core. Macromolecules 40, 7633-7637.

EMA/CHMP/ICH/82260/2006 Committee for Human Medicinal Products ICH guideline Q3C on impurities: guideline for residual solvents, 2019, European Medicines Agency.

Fessi, H., Puisieux, F., Devissaguet, J.P., Ammoury, N., Benita, S., 1989. Nanocapsule formation by interfacial polymer deposition following solvent displacement. Int. J. Pharm. 55, R1-R4.

Ghoroghchian, P.P., Li, G., Levine, D.H., Davis, K.P., Bates, F.S., Hammer, D.A., Therien, M.J., 2006. Bioresorbable Vesicles Formed through Spontaneous Self-Assembly of Amphiphilic Poly(ethylene oxide)-block-polycaprolactone. Macromolecules 39, 1673-1675.

Giacomelli, C., Borsali, R., 2006. Morphology of poly(ethylene oxide)-block-polycaprolatone block copolymer micelles controlled via the preparation method. Macromol. Symp. 245, 147-153.

Gref, R., Minamitake, Y., Peracchia, M.T., Trubetskoy, V., Torchilin, V., Langer, R., 1994. Biodegradable long-circulating polymeric nanospheres. Science 263, 1600-1603.

Günday Türeli, N., Türeli, A.E., Schneider, M., 2016. Optimization of ciprofloxacin complex loaded PLGA nanoparticles for pulmonary treatment of cystic fibrosis infections: Design of experiments approach. Int. J. Pharm. 515, 343-351.

Hannecart, A., Stanicki, D., Vander Elst, L., Muller, R.N., Brulet, A., Sandre, O., Schatz, C., Lecommandoux, S., Laurent, S., 2019. Embedding of superparamagnetic iron oxide nanoparticles into membranes of well-defined poly(ethylene oxide)-block-poly(epsilon-caprolactone) nanoscale magnetovesicles as ultrasensitive MRI probes of membrane bio-degradation. J. Mater. Chem. B 7, 4692-4705.

Hayward, R.C., Pochan, D.J., 2010. Tailored Assemblies of Block Copolymers in Solution: It Is All about the Process. Macromolecules 43, 3577-3584.

Hoshyar, N., Gray, S., Han, H., Bao, G., 2016. The effect of nanoparticle size on in vivo pharmacokinetics and cellular interaction. Nanomedicine (Lond.) 11, 673-692.

Johnson, B.K., Prud'homme, R.K., 2003. Mechanism for rapid self-assembly of block copolymer nanoparticles. Phys. Rev. Lett. 91, 118302.

Lavino, A.D., Di Pasquale, N., Carbone, P., Marchisio, D.L., 2017. A novel multiscale model for the simulation of polymer flash nano-precipitation. Chem. Eng. Sci. 71, 485-494.

Lebouille, J. G. J. L., Stepanyan, R., Slot, J.J.M., Cohen Stuart, M.A., Tuinier, R., 2014. Nanoprecipitation of polymers in a bad solvent. Colloids Surf., A 460, 225-235.

Lim Soo, P., Lovric, J., Davidson, P., Maysinger, D., Eisenberg, A., 2005. Polycaprolactone-block-poly(ethylene oxide) Micelles: A Nanodelivery System for 17β-Estradiol. Mol. Pharmaceutics 2, 519-527.

Lin, F., Cheng, C., Chuang, Y., Tung, S., 2018. Polymersomes with high loading capacity prepared by direct self-assembly of block copolymers in drugs. Polymer 134, 117-124.

Lince, F., Marchisio, D.L., Barresi, A.A., 2008. Strategies to control the particle size distribution of poly-ε-caprolactone nanoparticles for pharmaceutical applications. J. Colloid Interface Sci. 322, 505-515.

Liu, J., Gan, Z., 2014. Hydrophilic Block Azidation of PCL-b-PEO Block Copolymers from Epichlorohydrin. Macromol. Biosci. 14, 699-708.

Liu, Y., Yang, G., Zou, D., Hui, Y., Nigam, K., Middelberg, A.P.J., Zhao, C., 2020. Formulation of Nanoparticles Using Mixing-Induced Nanoprecipitation for Drug Delivery. Ind. Eng. Chem. Res. 59, 4134-4149.

Mai, Y., Eisenberg, A., 2012. Self-assembly of block copolymers. Chem. Soc. Rev. 41, 5969–5985.

Martínez Rivas, C.J., Tarhini, M., Badri, W., Miladi, K., Greige-Gerges, H., Nazari, Q.A., Galindo Rodríguez, S.A., Román, R.Á, Fessi, H., Elaissari, A., 2017. Nanoprecipitation process: From encapsulation to drug delivery. Int. J. Pharm. 532, 66-81.

Miladi, K., Sfar, S., Fessi, H., Elaissari, A., 2016. Nanoprecipitation Process: From Particle Preparation to In Vivo Applications. In: Vauthier, C., Ponchel, G. (Eds.), Polymer Nanoparticles for Nanomedicines: A Guide for their Design, Preparation and Development, Springer International Publishing, Cham, pp. 17-53.

Mohamadpour, H., Azadi, A., Rostamizadeh, K., Andalib, S., Saghatchi Zanjani, M.R., Hamidi, M., 2020. Preparation, Optimization, and Evaluation of Methoxy Poly(ethylene glycol)-co-Poly(ε-caprolactone) Nanoparticles Loaded by Rivastigmine for Brain Delivery. ACS Chem. Neurosci. 11, 783-795.

Montazeri Aliabadi, H., Brocks, D.R., Lavasanifar, A., 2005. Polymeric micelles for the solubilization and delivery of cyclosporine A: pharmacokinetics and biodistribution. Biomaterials 26, 7251-7259.

Park, M., Jun, S., Kim, I., Jin, S., Kim, J., Shin, T.J., Lee, E., 2015. Stepwise Drug-Release Behavior of Onion-Like Vesicles Generated from Emulsification-Induced Assembly of Semicrystalline Polymer Amphiphiles. Adv. Funct. Mater. 25, 4570-4579.

Park, Y.J., Lee, J.Y., Chang, Y.S., Jeong, J.M., Chung, J.K., Lee, M.C., Park, K.B., Lee, S.J., 2002. Radioisotope carrying polyethylene oxide–polycaprolactone copolymer micelles for targetable bone imaging. Biomaterials 23, 873-879.

Patel, S.K., Lavasanifar, A., Choi, P., 2009. Roles of Nonpolar and Polar Intermolecular Interactions in the Improvement of the Drug Loading Capacity of PEO-b-PCL with Increasing PCL Content for Two Hydrophobic Cucurbitacin Drugs. Biomacromolecules 10, 2584-2591.

Qi, W., Ghoroghchian, P.P., Li, G., Hammer, D.A., Therien, M.J., 2013. Aqueous self-assembly of poly(ethylene oxide)-block-poly(ε-caprolactone) (PEO-b-PCL) copolymers: disparate diblock copolymer compositions give rise to nano- and meso-scale bilayered vesicles. Nanoscale 5, 10908-10915.

Rajagopal, K., Mahmud, A., Christian, D.A., Pajerowski, J.D., Brown, A.E.X., Loverde, S.M., Discher, D.E., 2010. Curvature-Coupled Hydration of Semicrystalline Polymer Amphiphiles Yields flexible Worm Micelles but Favors Rigid Vesicles: Polycaprolactone-Based Block Copolymers. Macromolecules 43, 9736-9746.

Rowe, R.C., Sheskey, P.J., Quinn, M.E., 2009. Handbook of Pharmaceutical Excipients, 6th Ed., Pharmaceutical Press, London.

Ryu, J., Jeong, Y., Kim, I., Lee, J., Nah, J., Kim, S., 2000. Clonazepam release from core-shell type nanoparticles of poly(ε-caprolactone)/poly(ethylene glycol)/poly(ε-caprolactone) triblock copolymers. Int. J. Pharm. 200, 231-242.

Saad, W.S., Prud'homme, R.K., 2016. Principles of nanoparticle formation by flash nanoprecipitation. Nano Today 11, 212-227.

Shi, B., Fang, C., You, M.X., Zhang, Y., Fu, S., Pei, Y., 2005. Stealth MePEG-PCL micelles: effects of polymer composition on micelle physicochemical characteristics, in vitro drug release, in vivo pharmacokinetics in rats and biodistribution in S180 tumor bearing mice. Colloid Polym. Sci. 283, 954-967.

Sui, X., Kujala, P., Janssen, G., de Jong, E., Zuhorn, I.S., van Hest, Jan C. M., 2015. Robust formation of biodegradable polymersomes by direct hydration. Polym. Chem. 6, 691-696.

Tahir, N., Madni, A., Balasubramanian, V., Rehman, M., Correia, A., Kashif, P.M., Mäkilä, E., Salonen, J., Santos, H.A., 2017. Development and optimization of methotrexate-loaded lipid-polymer hybrid nanoparticles for controlled drug delivery applications. Int. J. Pharm. 533, 156-168.

Villamil, J.C., Parra-Giraldo, C.M., Perez, L.D., 2019. Enhancing the performance of PEG-b-PCL copolymers as precursors of micellar vehicles for amphotericin B through its conjugation with cholesterol. Colloids Surf., A 572, 79-87.

Werner, M.E., Cummings, N.D., Sethi, M., Wang, E.C., Sukumar, R., Moore, D.T., Wang, A.Z., 2013. Preclinical Evaluation of Genexol-PM, a Nanoparticle Formulation of Paclitaxel, as a Novel Radiosensitizer for the Treatment of Non-Small Cell Lung Cancer. Int. J. Radiat. Oncol., Biol., Phys. 86, 463-468.

Woodruff, M.A., Hutmacher, D.W., 2010. The return of a forgotten polymer—Polycaprolactone in the 21st century. Prog. Polym. Sci. 35, 1217-1256.

Yang, J., Hou, Y., Ji, G., Song, Z., Liu, Y., Dai, G., Zhang, Y., Chen, J., 2014. Targeted delivery of the RGD-labeled biodegradable polymersomes loaded with the hydrophilic drug oxymatrine on cultured hepatic stellate cells and liver fibrosis in rats. Eur. J. Pharm. Sci. 52, 180-190.

Zhou, J., Ni, R., Chau, Y., 2017. Polymeric vesicle formation via temperature-assisted nanoprecipitation. RSC Adv. 7, 17997-18000.

Zou, T., Dembele, F., Beugnet, A., Sengmanivong, L., Trepout, S., Marco, S., de Marco, A., Li, M., 2015. Nanobody-functionalized PEG-b-PCL polymersomes and their targeting study. J. Biotechnol. 214, 147-155.

Supporting information

Evaluation of the effects of nanoprecipitation process parameters on the size and morphology of poly(ethylene oxide)-*block*-polycaprolactone nanostructures

Voitto Känkänen[a], Jani Seitsonen[b], Henri Tuovinen[a], Janne Ruokolainen[b], Jouni Hirvonen[a], Vimalkumar Balasubramanian[c]*, Hélder A. Santos[a,d,]*

[a] Drug Research Program, Division of Pharmaceutical Chemistry and Technology, Faculty of Pharmacy, University of Helsinki, FI-00014 Helsinki, Finland

[b] Nanomicroscopy Center, Aalto University, Puumiehenkuja 2, FI-02150 Espoo, Finland

[c] Chemical and Pharmaceutical Development, Bayer Oy, FI-20210 Turku, Finland

[d] Helsinki Institute of Life Science (HiLIFE), University of Helsinki, FI-00014 Helsinki, Finland

Table S1. Manufacturing parameters used for DoE study.

Run	Whole plots	Subplots	Stirring speed (rpm)	Polymer concentration (mg/mL)	Organic phase addition rate (mL/h)	Organic phase volume (mL)
1	1	1	800	6	250	0.738
2	1	1	800	6	10	1.600
3	1	1	800	6	10	0.480
4	1	2	800	20	250	0.480
5	1	2	800	20	130	1.600
6	1	2	800	20	10	0.480
7	2	3	120	20	10	0.480
8	2	3	120	20	250	0.738
9	2	3	120	20	10	1.600
10	2	4	120	6	250	1.600
11	2	4	120	6	10	0.738
12	2	4	120	6	250	0.480
13	3	5	800	20	10	0.738
14	3	5	800	20	250	1.600
15	3	5	800	20	250	0.480
16	3	6	800	13	130	0.480
17	3	6	800	13	10	1.600
18	3	6	800	13	250	1.600
19	4	7	460	6	130	1.600
20	4	7	460	6	10	0.480
21	4	7	460	6	250	0.480
22	4	8	460	13	10	1.600
23	4	8	460	13	250	1.600
24	4	8	460	13	130	0.738

Table S2. Preparation parameters of samples for cryo-TEM analysis, where ***T*** is the precipitation temperature, $\boldsymbol{\phi_W}$ is the water volume fraction, $\boldsymbol{c_P}$ is the concentration of polymer in organic phase, ***S*** is the stirring rate and ***A*** is the addition rate of organic phase to water.

Polymer	$\boldsymbol{f_{PEO}}$	***T***	**Water vol. (mL)**	**Organic vol. (mL)**	$\boldsymbol{\phi_W}$	$\boldsymbol{c_P}$ **(mg/mL)**	***S*** **(rpm)**	***A*** **(mL/h)**
PEO_{113}-*b*-PCL_{101}	0.29	R.T.	1.200	1.800	0.4	10	400	200
PEO_{113}-*b*-PCL_{101}	0.29	R.T.	1.200	0.982	0.55	10	400	200
PEO_{113}-*b*-PCL_{101}	0.29	R.T.	1.200	0.514	0.7	10	400	200
PEO_{113}-*b*-PCL_{101}	0.29	65 °C	1.200	0.514	0.7	10	400	200
PEO_{113}-*b*-PCL_{44}	0.48	R.T.	1.200	1.800	0.4	10	400	200
PEO_{113}-*b*-PCL_{44}	0.48	R.T.	1.200	0.982	0.55	10	400	200
PEO_{113}-*b*-PCL_{44}	0.48	R.T.	1.200	0.514	0.7	10	400	200
PEO_{113}-*b*-PCL_{44}	0.48	65 °C	1.200	0.514	0.7	10	400	200
PEO_{45}-*b*-PCL_{88}	0.16	R.T.	1.200	0.514	0.7	10	400	200
PEO_{45}-*b*-PCL_{88}	0.16	65 °C	1.200	0.514	0.7	10	400	200
PEO_{45}-*b*-PCL_{12}	0.57	R.T.	1.200	0.514	0.7	10	400	200
PEO_{45}-*b*-PCL_{12}	0.57	65 °C	1.200	0.514	0.7	10	400	200
PEO_{45}-*b*-PCL_{9}	0.65	R.T.	1.200	0.514	0.7	10	400	200
PEO_{45}-*b*-PCL_{9}	0.65	65 °C	1.200	0.514	0.7	10	400	200

Table S3. Pearson correlation coefficients and corresponding p-values between variables. The data set includes polymer samples PEO_{113}-b-PCL_{219}, PEO_{113}-b-PCL_{101}, PEO_{113}-b-PCL_{44} and PEO_{45}-b-PCL_{88}.

	Correlations							
	N	f_{PEO}	S	c_P	A	ϕ_W	d_H	PDI
N	1.000	−0.5906	0.0000	0.0000	−0.0000	−0.0018	0.6473	−0.5347
f_{PEO}	−0.5906	1.000	0.0000	−0.0000	0.0000	0.0014	−0.4673	0.2553
S	0.0000	0.0000	1.000	0.1741	−0.0000	−0.0104	−0.1122	0.0836
c_P	0.0000	−0.0000	0.1741	1.000	−0.0000	−0.0020	0.0513	0.0993
A	−0.0000	0.0000	−0.0000	−0.0000	1.000	0.0014	−0.0422	−0.0226
ϕ_W	−0.0018	0.0014	−0.0104	−0.0020	0.0014	1.000	−0.1864	−0.4497
d_H	0.6473	−0.4673	−0.1122	0.0513	−0.0422	−0.1864	1.000	0.0422
PDI	−0.5347	0.2553	0.0836	0.0993	−0.0226	−0.4497	0.0422	1.000
	Correlation p-values							
	N	f_{PEO}	S	c_P	A	ϕ_W	d_H	PDI
N	<0.0001	<0.0001	1.0000	1.0000	1.0000	0.9816	<0.0001	<0.0001
f_{PEO}	<0.0001	<0.0001	1.0000	1.0000	1.0000	0.9861	<0.0001	0.0008
S	1.0000	1.0000	<0.0001	0.0240	1.0000	0.8939	0.1474	0.2814
c_P	1.0000	1.0000	0.0240	<0.0001	1.0000	0.9790	0.5094	0.2002
A	1.0000	1.0000	1.0000	1.0000	<0.0001	0.9855	0.5874	0.7716
ϕ_W	0.9816	0.9861	0.8939	0.9790	0.9855	<0.0001	0.0155	<0.0001
d_H	<0.0001	<0.0001	0.1474	0.5094	0.5874	0.0155	<0.0001	0.5872
PDI	<0.0001	0.0008	0.2814	0.2002	0.7716	<0.0001	0.5872	<0.0001

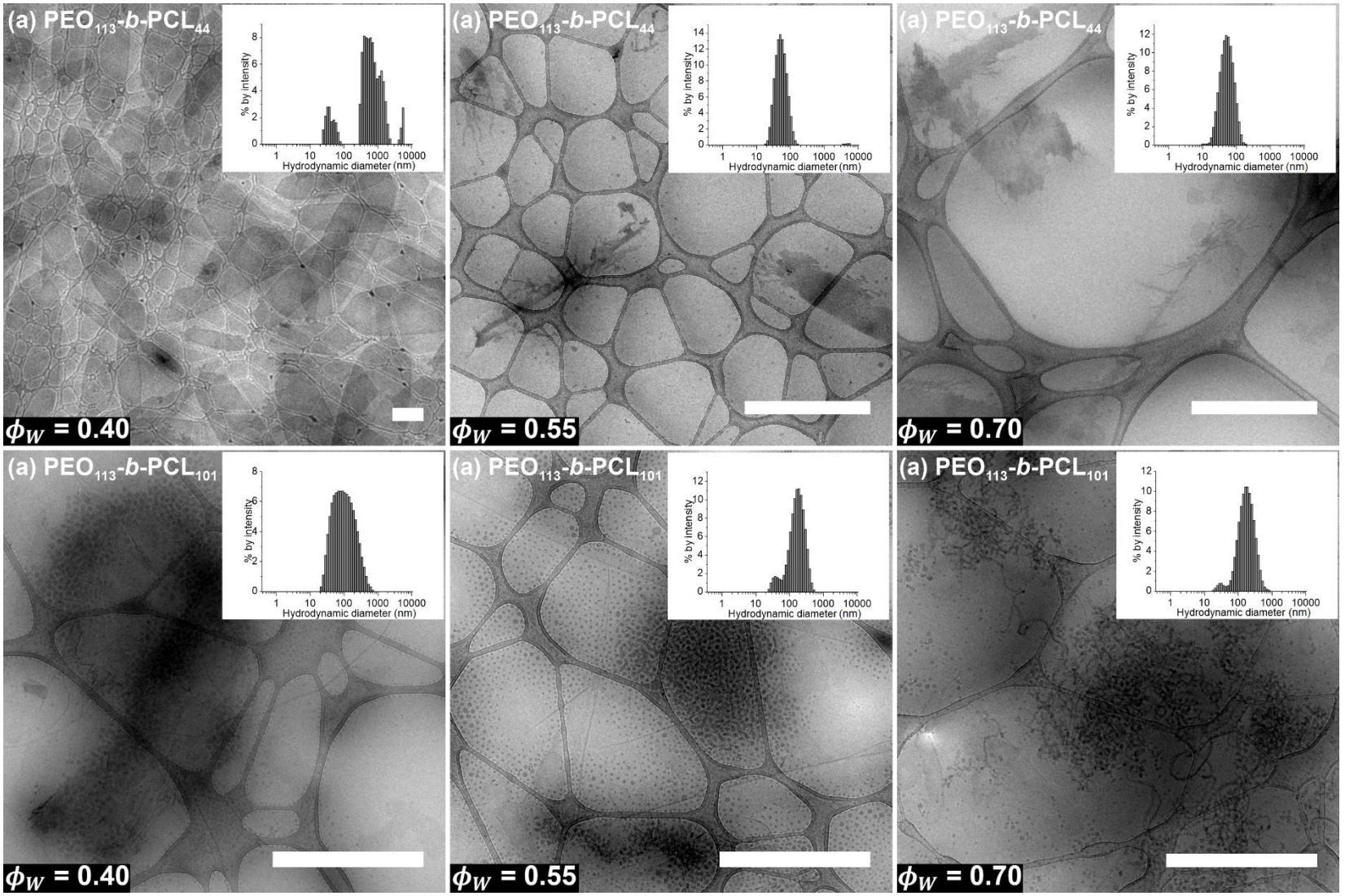

Figure S1. Low-magnification micrographs of samples prepared with different values of water volume fraction ϕ_W, showing the micron-scale structures. Size distributions obtained by dynamic light scattering are presented in inserts. Scale bars are 1 μm.

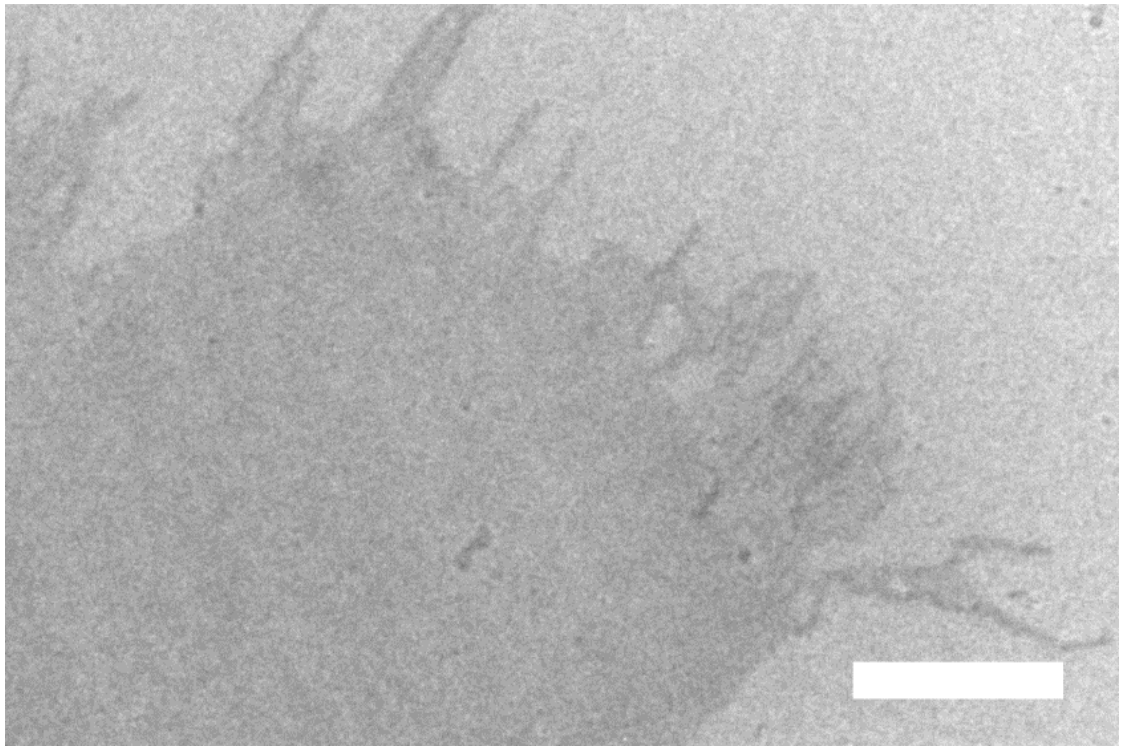

Figure S2. High-magnification of a large object seen in low water fraction ($\phi_W = 0.40$) sample of PEO_{113}-b-PCL_{44}. Scale bar is 200 nm.

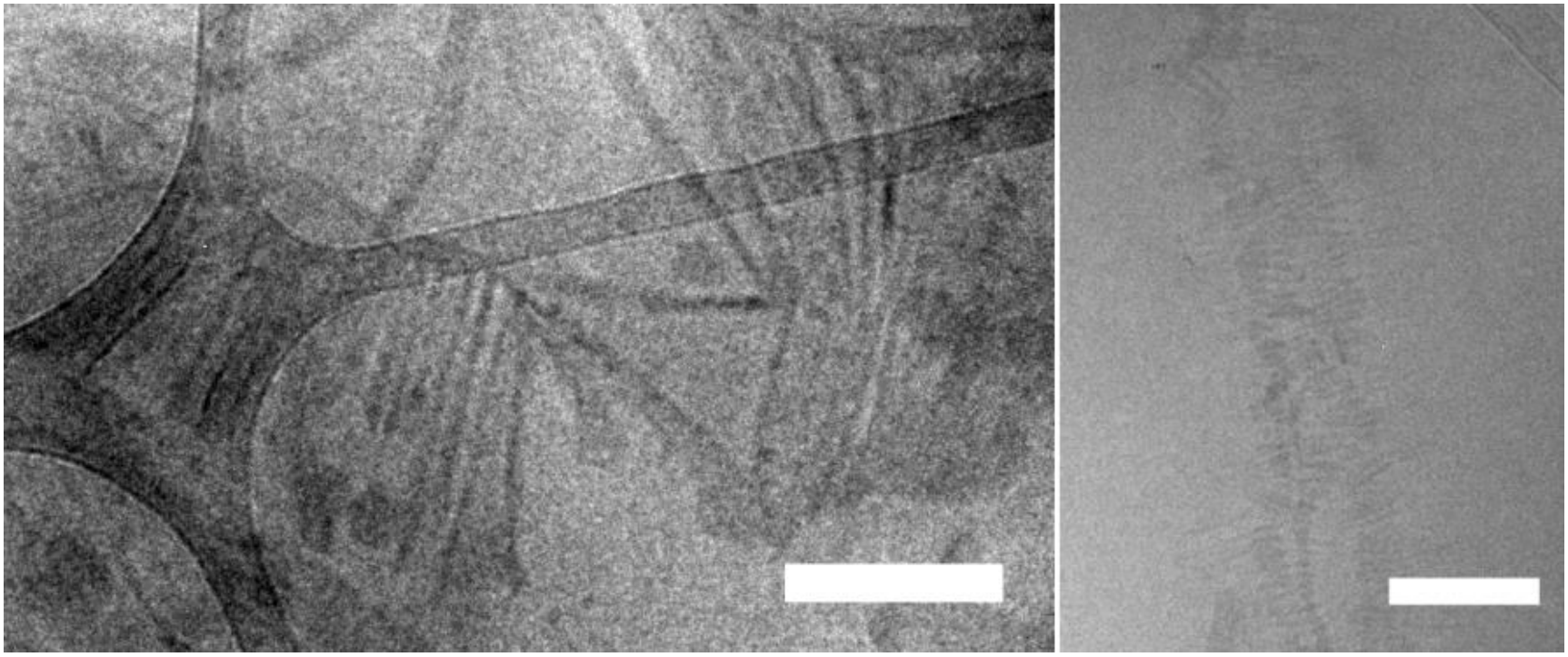

Figure S3. Cryo-TEM micrographs of lamellar and ladder-like structures discovered in high-temperature nanoprecipitation sample of PEO_{45}-b-PCL_{88}. Scale bars are 200 nm.

Table S4. Coefficients of linear regression model based on PEO_{113}-b-PCL_{219} data set.

Response	Coefficients	Intercept	ϕ_W	c_P	S	A
d_H	Standardized	+180.4	-1.64×10^{1}	$+2.51 \times 10^{1}$	-2.11×10^{1}	−2.55
	Absolute	+222.7	-1.03×10^{2}	+3.59	-6.22×10^{-2}	-2.12×10^{-2}
PDI	Standardized	+0.161	$+1.15 \times 10^{-2}$	$+7.30 \times 10^{-3}$	-9.38×10^{-3}	-3.86×10^{-3}
	Absolute	+0.124	$+7.20 \times 10^{-2}$	$+1.04 \times 10^{-3}$	-2.76×10^{-5}	-3.21×10^{-5}

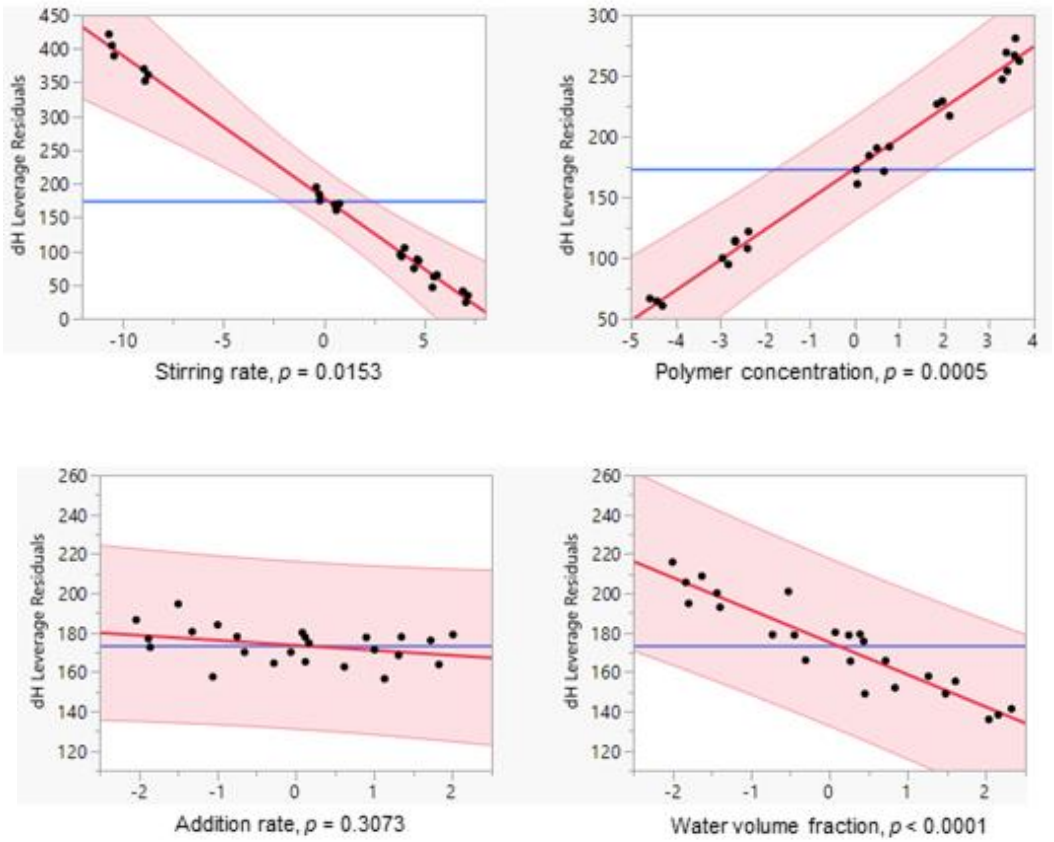

Figure S4. Leverage plots of the linear regression model for d_H showing the effects of each process variable. Plots were created using the Fit Model function of JMP Pro 14.

Table S5. Coefficients of full quadratic models based on PEO_{113}-b-PCL_{219} data set.

Response	Coefficients	Int.	ϕ_W	c_P	S	A	ϕ_W^2	c_P^2	S^2	A^2	$\phi_W c_P$	$\phi_W S$	$\phi_W A$	$c_P S$	$c_P A$	SA
d_H	Standardized	+174.5	-1.62×10^{1}	$+2.32 \times 10^{1}$	-2.01×10^{1}	−4.14	+1.91	-6.60×10^{-1}	−1.56	+7.58	+1.91	+2.47	+4.26	−2.69	−1.53	+6.41
	Absolute	+286.7	-2.57×10^{2}	+3.47	-7.79×10^{-2}	-3.44×10^{-1}	$+7.47 \times 10^{1}$	-1.35×10^{-2}	-1.35×10^{-5}	$+5.26 \times 10^{-4}$	+1.70	$+4.53 \times 10^{-2}$	$+2.22 \times 10^{-1}$	-1.13×10^{-3}	-1.83×10^{-3}	$+1.57 \times 10^{-4}$
PDI	Standardized	+0.142	$+4.09 \times 10^{-3}$	$+1.09 \times 10^{-2}$	-2.03×10^{-3}	-6.14×10^{-3}	-5.86×10^{-3}	$+1.78 \times 10^{-2}$	$+6.31 \times 10^{-3}$	$+8.80 \times 10^{-3}$	-1.10×10^{-2}	$+1.71 \times 10^{-2}$	$+1.63 \times 10^{-2}$	-3.57×10^{-2}	-1.28×10^{-2}	$+9.99 \times 10^{-3}$
	Absolute	$+9.89 \times 10^{-2}$	$+1.55 \times 10^{1}$	$+6.50 \times 10^{-3}$	-6.87×10^{-5}	-6.00×10^{-4}	-2.29×10^{-1}	$+3.63 \times 10^{-4}$	$+5.46 \times 10^{-8}$	$+6.11 \times 10^{-7}$	-9.82×10^{-3}	$+3.13 \times 10^{-4}$	$+8.51 \times 10^{-4}$	-1.50×10^{-5}	-1.53×10^{-5}	$+2.45 \times 10^{-7}$

Table S6. Coefficients of simplified quadratic models based on PEO_{113}-b-PCL_{219} data set.

Response	Coefficients	Int.	ϕ_W	c_P	S	A	A^2	$\phi_W c_P$	$\phi_W S$	$\phi_W A$	$c_P S$	$c_P A$	SA
d_H	Standardized	+177.0	-1.66×10^{1}	$+2.37 \times 10^{1}$	-2.06×10^{1}	−4.09	+4.35	--	+2.66	+4.25	−2.72	--	+6.02
	Absolute	+259.4	-1.55×10^{2}	+3.91	-9.24×10^{-2}	-3.05×10^{-1}	$+3.02 \times 10^{-4}$	--	$+4.88 \times 10^{-2}$	$+2.22 \times 10^{-1}$	-1.14×10^{-3}	--	$+1.48 \times 10^{-4}$
PDI	Standardized	+0.164	$+7.73 \times 10^{-3}$	$+1.40 \times 10^{-2}$	-4.22×10^{-3}	-5.89×10^{-3}	--	-1.12×10^{-2}	$+1.51 \times 10^{-2}$	$+1.62 \times 10^{-2}$	-3.41×10^{-2}	-1.26×10^{-2}	$+1.05 \times 10^{-2}$
	Absolute	$+8.94 \times 10^{-2}$	-5.88×10^{-2}	$+1.60 \times 10^{-2}$	$+1.50 \times 10^{-5}$	-4.47×10^{-4}	--	-1.00×10^{-2}	$+2.77 \times 10^{-4}$	$+8.46 \times 10^{-4}$	-1.43×10^{-5}	-1.50×10^{-5}	$+2.58 \times 10^{-7}$

Table S7. Coefficients of simplified quadratic models with polymerization degree included as predictor for $f_{PEO} = 0.16$ polymers.

Response	Coefficients	Intercept	N	ϕ_W	c_P	S	ϕ_W^2	Nc_P	NS	$N\phi_W$	$c_P\phi_W$
d_H	Standardized	+126.6	$+5.32 \times 10^{1}$	-1.02×10^{1}	+8.14	−8.61	$+1.24 \times 10^{1}$	1.26×10^{1}	-1.21×10^{1}	--	+6.98
	Absolute	+247.9	$+4.62 \times 10^{-1}$	-8.51×10^{1}	−6.56	$+5.77 \times 10^{-2}$	$+4.82 \times 10^{2}$	$+1.82 \times 10^{-2}$	-3.57×10^{-4}	--	+6.23
PDI	Standardized	+0.245	-1.19×10^{-1}	-5.11×10^{-2}	--	--	$+6.59 \times 10^{-2}$	--	-3.03×10^{-2}	$+6.62 \times 10^{-2}$	--
	Absolute	+1.956	-3.12×10^{-3}	−4.17	--	--	2.58	--	-8.97×10^{-7}	$+4.16 \times 10^{-2}$	--